# Investigation of 3D Printed Underwater Thruster Propellers Using CFD and Structural Simulations

Krisztián Kiss-Nagy[1*], Győző Simongáti[1], Péter Ficzere[2]

[1] Department of Aeronautics and Naval Architecture, Faculty of Transportation Engineering and Vehicle Engineering, Budapest University of Technology and Economics, Műegyetem rkp. 3., H-1111 Budapest, Hungary
[2] Department of Railway Vehicles and Vehicle System Analysis, Faculty of Transportation Engineering and Vehicle Engineering, Budapest University of Technology and Economics, Műegyetem rkp. 3., H-1111 Budapest, Hungary
* Corresponding author, e-mail: kiss-nagy.krisztian@edu.bme.hu

## Abstract

Unmanned Surface Vehicles (USV) and Autonomous or Remotely Operated Underwater vehicles (AUV, ROV) are developing and spreading rapidly in various industries. A common feature of these vehicles is that they are propelled by small plastic (or metal) propellers in most cases. Additive manufacturing can offer an excellent opportunity for rapid prototyping and the development of new models. This paper aims to investigate the fundamental aspects to be considered in the geometric design and manufacturing of small (diameter less than 100 mm) PLA (Polylactic acid) propellers 3D-printed using Fused Filament Fabrication (FFF) technology. In-service deformation of 3D-printed PLA ducted propellers with average geometry was investigated to determine the effect on the thrust and torque on the blades. For this purpose, one-directional FSI (Fluid Solid Interaction) simulations were performed using CFD (Computational Fluid Dynamics) and structural simulations. The propeller CAD geometries were generated using an in-house MATLAB script. The variable parameters of each version are the thickness, skew, and rake of the propeller blades. For the structural simulations, it was considered that the material properties of PLA parts printed with FFF technology depend on the print orientation. The results of the simulations show that except for extreme geometries (e.g., thin blades, skew, or rake more than 10°), the deformation of small PLA ducted propellers is not significant. CFD studies of the deformed geometries have shown that the resulting deformation has no significant effect on the thrust and torque of the propeller and thruster.

## Keywords

3D-printed propeller, rapid prototyping, PLA propellers, CFD, FEM

## 1 Introduction

Nowadays, Unmanned Surface Vehicles (USVs), Autonomous Underwater Vehicles (AUVs), and Remotely Operated Vehicles (ROVs) are becoming increasingly common, providing a great help for safe, sustainable, and cost-effective marine and inland waterway operations. Typical tasks, based on the studies so far, include seabed and river bed mapping [1], water quality measurement and monitoring [2], current velocity and sediment volume measurement [3], underwater environment monitoring, construction, maintenance and monitoring of underwater structures [4], which are dangerous, costly, boring or impractical (e.g. human presence interferes with measurements). These surface or underwater vehicles are almost always propelled by small marine propellers (average diameter 100 mm), which can be ducted. In most cases,

USVs and ROVs are equipped with thrusters, as in studies such as [5–7]. An interesting development has been carried out by [8], in which a small size and high-efficiency plastic counter-rotating thruster has been implemented to propel ROVs. Direct drive ducted propeller has been investigated on AUVs, for example [9], or a free propeller has been used, for example [10]. In [11], a positive buoyancy diving autonomous vehicle was fitted with a ducted thruster to combine the features of a USV and an AUV. These propellers are typically made of plastic, as metal propellers are much more expensive and difficult to manufacture. If propellers for prototypes or small series USVs, ROVs or AUVs need to be manufactured, there is an opportunity to use additive manufacturing (AM). There are many examples of USVs being equipped with 3D-printed propellers.

For example, [12] used an innovative PLA propeller for a 3SCH (Three Slender Cylinders Hull) USV, which gave the USV higher speed. A small-scale, low-cost water quality measurement USV was developed by [13] using 3D-printed underwater thrusters. Additive manufacturing technology is also becoming popular in other areas. For example, [14] investigated small 3D-printed LW-PLA (Lightweight polylactic acid) propellers and compared the thrust of surface-treated and untreated PLA propellers. In [15], a study on material selection of drone propellers was conducted based on a strength analysis comparison of 3D-printed propellers made of ABS, PETG and PLA materials. As a result of this research, PETG material was selected. Useful research has been carried out by [16] with 3D-printed PLA propellers to investigate the effect of printing settings on strength and propulsion properties. As a result of the research, with the right print settings, the propulsion properties will be close to those of conventional injection molded propellers, but the strength properties will be less, making this technology good for initial prototype testing but not yet suitable for mass production.

This paper investigates the fundamental aspects to be considered in the geometric design and manufacturing of small PLA propellers 3D-printed using Fused Filament Fabrication (FFF) technology. The study will investigate the impact of in-service deformation of 3D-printed PLA ducted propellers on the thrust and torque acting on the blades. For this purpose, CFD (Computational Fluid Dynamics) analyses and structural simulations have been carried out, considering the anisotropic (orthotropic) properties of PLA parts printed with FFF technology.

There are many methods for CFD analysis of propellers. For example, [17] used SM-Sliding Mesh (or AMI-Arbitrary Mesh Interface) to model the propeller of an underwater thruster and could simulate the maneuverability of an AUV with good results. Another study [18] compared the MRF-Moving Reference Frame and SM methods and concluded that the SM method provides more accurate data on the propeller but requires more computation time.

Coupled fluid flow and strength simulations (FSI-Fluid Solid Interaction, or Hydroelastic) on composite propellers have been performed by [19–21], highlighting that composite propellers suffer higher deformations than metal ones, but their application can drastically reduce vibration. In [22], a design method has been developed that uses bidirectional FSI simulation to perform geometric optimization of propellers to increase thrust and strength.

To perform a strength simulation based on the CFD results, it is necessary to know the properties of the propeller material, which considers not only the PLA filament strength characteristic but also the specificities of the FFF technology. For this purpose, PLA test specimens have been investigated in [23–25] to determine the material properties of parts printed with FFF technology by considering that the material properties depend on the printing orientation. Similar studies were performed by [26] with the addition of comparing the properties of conventional PLA and PLA-CF (carbon fiber reinforced filament) test specimens and concluded that PLA-CF is stronger at certain orientations and print settings but weaker than conventional PLA at other settings or orientations, and therefore only offers an advantage in special cases. An interesting topic was investigated in [27], where finite element analysis of 3D-printed components was carried out with special attention to their inherent strains.

## 2 Geometry

The geometry of the investigated propellers has been generated using an in-house developed MATLAB [28] code. Following the recommendations of [29], the program uses a modified NACA 66 profile thickness distribution, and a camber distribution marked $a = 0.8$. The parameters that can be varied during the automatic profile generation are the chord length ($c$), the maximum thickness ($t_{max}$), and the maximum distance of the camber line from the chord ($f_{max}$), as shown in Fig. 1:

Diameter ($D = 2R$), pitch ratio ($P/D$), blade area ratio ($A_E/A_O$), number of blades ($z$), Rake and Skew can be adjusted as shown in Fig. 2. The radial distribution of the propeller characteristics can be adjusted by moving the control points of the Bézier curves for parameterizability, ease of adjustment and continuous transitions. This allows the creation of 6 functions which set the following parameters:

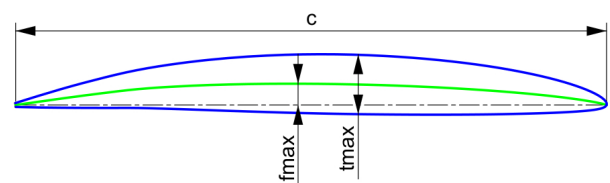- Each profile's pitch along the radius normalized by the "global" pitch ($P_r/P$).



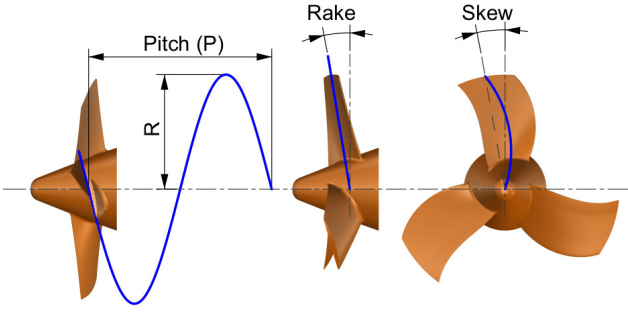**Fig. 1** Propeller blade profile parameters

**Fig. 2** Pitch, Rake and Skew parameters

- Each profile's rake along the radius normalized by the "global" rake ($Rake_r/Rake$).
- Skew of each profile along the radius in degrees (Skew).
- Radial distribution of profile chord length ($c$) normalized by the propeller width coefficient ($W_{mid}$).
- Radial distribution of the maximum profile thickness ($t_{max}$) normalized by the blade tip maximum profile thickness ($t_{tip}$) ($t_{max}/t_{tip}$).
- Radial distribution of the maximum profile thickness ($t_{max}$) normalized by the maximum profile deflection ($f_{max}$) ($t_{max}/f_{max}$).

The propeller width coefficient $W_{mid}$ is defined in Eq. (1).

$$W_{mid} = \text{Width}_c \times \frac{1}{z} \times A_E / A_O \times D \qquad (1)$$

Where $\text{Width}_c = 1.972$ is a dimensionless constant. Seven different propeller geometries were investigated to estimate the deformation dependence of FFF 3D-printed PLA propellers on the basic geometric parameters. The changing parameters were the maximum profile thickness measured at the maximum diameter ($t_{tip}$ [mm]), the ("constant") rake of the propeller (in degrees), and the maximum skew of the propeller (in degrees). Apart from these, all remaining propeller characteristics were constant. The three variable parameters were examined separately, not their combined effect. Considering this, the cases shown in Table 1 can be defined.

**Table 1** Parameters of the propeller variations

| Propeller No. | 1 | 2 | 3 | 4 | 5 | 6 | 7 |
|---|---|---|---|---|---|---|---|
| $D$ [mm] | | | | 65 | | | |
| $A_E/A_O$ [-] | | | | 0.4 | | | |
| $P/D$ [-] | | | | 0.8 | | | |
| $z$ [-] | | | | 3 | | | |
| $t_{tip}$ [mm] | 2 | 1.6 | 1.2 | 2 | 2 | 2 | 2 |
| Rake [deg] | 0 | 0 | 0 | 10 | 20 | 0 | 0 |
| Skew [deg] | 0 | 0 | 0 | 0 | 0 | 10 | 20 |

Fig. 3 shows the radial distribution of the propeller parameters, and since all parameters are dimensionless except for the skew of the propeller, they remain the same for all geometries. The comparison of the skew of the propellers is also shown in Fig. 3, together with the control points of the Bézier curves. The MATLAB code generates 3D blade section coordinates, which can be imported into the Rhinoceros software [30] to create the 3D CAD model of the propellers, as illustrated in Fig. 4.

Since the thrusters of USVs and ROVs are almost always equipped with ducted propellers, the propeller models were all tested in a nozzle with NACA6518 profile. The flow simulations also considered the electric motor housing and the supporting struts of the nozzle.

The dimensions of the computational domain and the propeller environment used for the CFD simulations are shown in Fig. 5. The MRF method was used
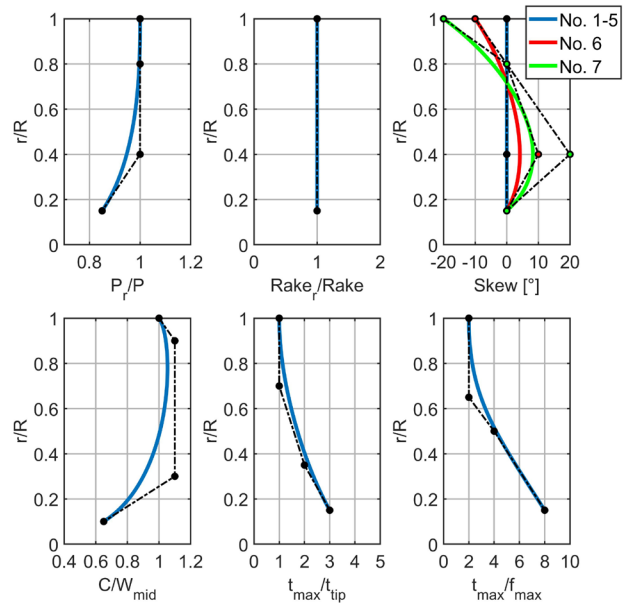


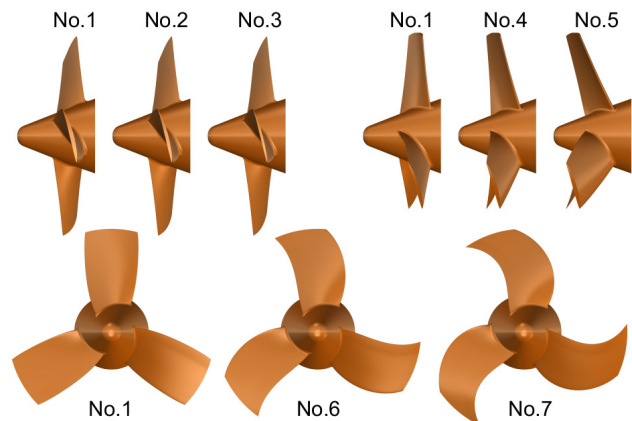**Fig. 3** Distribution of the propeller parameters along the radius
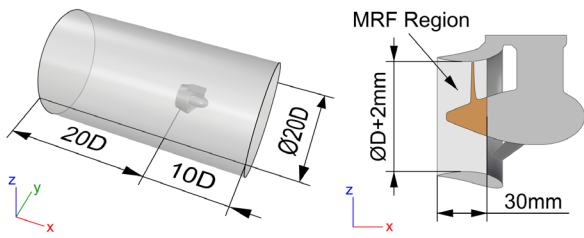


**Fig. 4** Propeller CAD models

**Fig. 5** Computational domain and MRF region dimensions

for the simulations (more details later), so the propeller and its surroundings were placed in a separate region (MRF Region).

## 3 Mesh

An unstructured tetrahedral mesh was used for the CFD simulations, illustrated in Fig. 6. The cells behind and around the thruster were refined. The No. 1 propeller was investigated with three different cell numbers (0.8 million, 1.5 million, and 4 million), and the results showed that the medium cell number of 1,441,762 is sufficient for accurate but cost-effective simulations.

For strength simulations, an unstructured tetrahedral mesh was also used. The cell size on the propeller surface is the same as the CFD mesh. The mesh is shown in Fig. 7, with an average cell number of about 50,000.
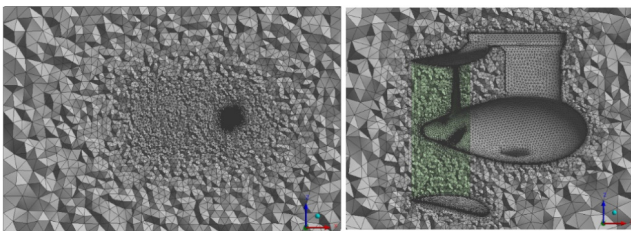


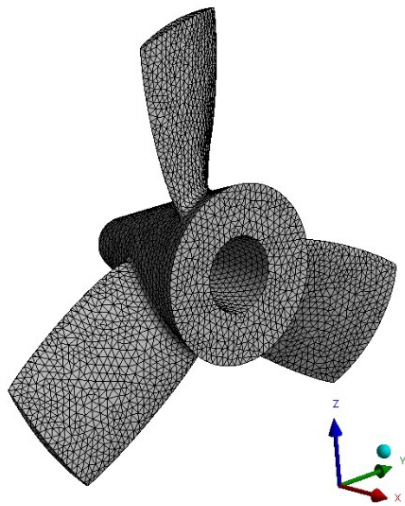**Fig. 6** XZ section views of the mesh



**Fig. 7** Structural FEM mesh of propeller No. 1

## 4 CFD model

During the CFD tests, the propeller speed was constant at 4000 rpm, and the advance speed was 0 m/s in all cases. Although this is not the typical operating condition of the propeller (since propellers on a USV are rarely used and only for short periods without the vessel moving), it was investigated because it is the most crucial case. This is the case when the highest thrust on the blades is applied, and therefore, the highest deformation is expected and the easiest to perform validation.

The simulations were carried out using Ansys Fluent CFD software [31]. Based on the related literature, the MRF method was used to model the propeller rotation because it provides a shorter simulation run time with sufficient accuracy compared to the Sliding Mesh or Overset Mesh methods. The SST $k$-$\omega$ turbulence model was used for turbulence modelling, and the time step was set to 0.005 s. The turbulence model applicability was checked using $y+$. The inlet of the outer (stationary) cylindrical flow field was defined as velocity inlet (flow velocity 0 m/s), the outlet as pressure outlet, and the cylinder wall was defined as symmetry boundary condition. The surface roughness of the propeller, nozzle, and motor casing was not considered.

It is very important to highlight that this study aims not to calculate the exact data of a specific propeller but to investigate the effect of the thrust and deformation on FFF 3D-printed PLA propellers with different geometries. Although 1.5 million cells may not be enough to accurately simulate propellers with high rotational speed, it has been used to ensure the cost-effective use of computer resources. The validation of the CFD model and the deformation values due to the hydrodynamic forces is planned and will be further investigated. A difficulty is to ensure proper surface quality since the surface of thin FFF 3D-printed propeller blades is very rough (stepped), but excessive surface treatment (e.g., epoxy coating and sanding) can affect the deformation.

## 5 Structural simulations

Ansys Mechanical software [32] was used for the strength (and unidirectional FSI) simulations. As a result of the literature research carried out in Section 1, it can be concluded that for accurate strength studies, it is essential to perform proper measurements for a given 3D-printer and material (PLA filament) to determine the material properties of PLA parts 3D-printed with FFF technology. It is important to emphasize that the present study aims not to obtain accurate deformation values but to characterize the expected changes in thrust

and torque of the propeller due to deformation based on average FFF 3D-printed PLA material properties. Considering that the layer thickness is 0.1 mm, the orthotropic material properties shown in Table 2 were used in the structural simulations. Poisson's ratios and shear elastic modulus were estimated from [33–36]. From Table 2, the material properties depend on the printing direction, whose dependence is mainly manifested in the tensile strength. The construction direction in the present case is the $x$-axis because when printing a propeller with more than two blades, the propeller axis must coincide with the construction direction. Otherwise, the strength properties of the blades would be different due to the slicing. The propeller load is the surface pressure distribution resulting from the CFD calculations, which the software interpolates to the structural mesh. An additional load is the constant angular rotational velocity of the propeller. As a constraint, the tapered bore for fixing the propeller to the motor shaft is fixed in all directions (Fixed Support).

## 6 Results

The individual propellers were first tested with the original geometry using CFD, and then the resulting surface pressure distribution was used as the load for the structural analyses. The resulting deformed geometry was exported to stl format, and the deformed CAD model (step format) was created using Rhinoceros software [30]. The deformed geometry was then re-examined using CFD with the same settings, resulting in a comparison of the resultant thrust on the thruster, thrust on the propeller, moment on the propeller, and maximum deformation and stress on the propeller for each propeller geometry. The steps in the process are illustrated in Fig. 8. The results are shown in Table 3, comparing the characteristics of the original and the deformed (def.) propeller. To show the differences, the relative deviations are shown in the diff. column. To illustrate the deformations, the distribution of the deformation of No. 1 and No. 7 propellers are shown in Fig. 9.
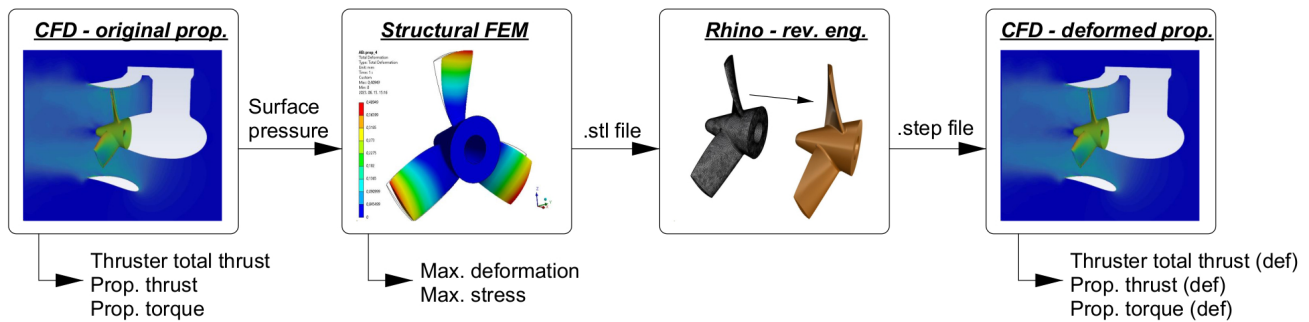
**Table 2** Material properties of FFF 3D-printed parts (building direction: $x$)

| Property | Unit | Value |
|---|---|---|
| (Layer height) | mm | 0.1 |
| Density | kg/m³ | 1.24 |
| Young's modulus X direction | MPa | 2444 |
| Young's modulus Y direction | MPa | 2864 |
| Young's modulus Z direction | MPa | 2864 |
| Poisson's ratio XY | - | 0.35 |
| Poisson's ratio YZ | - | 0.35 |
| Poisson's ratio XZ | - | 0.35 |
| Shear modulus XY | MPa | 1040 |
| Shear modulus YZ | MPa | 1040 |
| Shear modulus XZ | MPa | 1040 |
| Tensile strength X direction | MPa | 23.4 |
| Tensile strength Y direction | MPa | 49.6 |
| Tensile strength Z direction | MPa | 49.6 |



**Fig 8** Workflow of the one-way FSI simulations

**Table 3** Comparison of original and deformed propellers' thrust, torque, deformation and stress

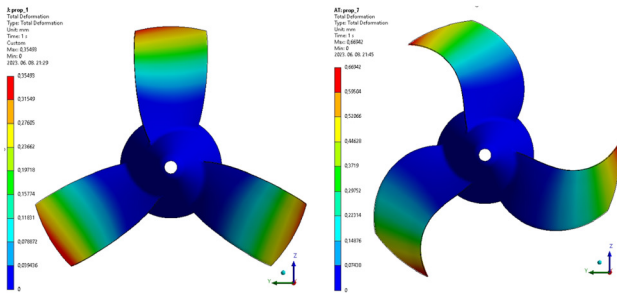| | Thruster total thrust [N] | | | Propeller thrust [N] | | | Propeller torque [Nm] | | | Max. deformation [mm] | Max. stress [MPa] |
|---|---|---|---|---|---|---|---|---|---|---|---|
| | | def. | diff. | | def. | diff. | | def. | diff. | | |
| No. 1 | 23.94 | 24.13 | +0.79% | 10.21 | 10.39 | +1.76% | −0.131 | −0.134 | +2.29% | 0.36 | 6.44 |
| No. 2 | 22.67 | 23.17 | +2.22% | 9.64 | 9.96 | +3.27% | −0.118 | −0.123 | +4.85% | 0.58 | 8.67 |
| No. 3 | 21.53 | 22.91 | +6.44% | 9.04 | 9.95 | +10.08% | −0.105 | −0.119 | +12.94% | 1.15 | 12.75 |
| No. 4 | 24.17 | 24.73 | +2.34% | 9.75 | 9.96 | +2.20% | −0.129 | −0.133 | +2.89% | 0.41 | 6.85 |
| No. 5 | 23.34 | 24.61 | +5.45% | 10.52 | 10.65 | +1.25% | −0.133 | −0.138 | +3.77% | 0.54 | 7.76 |
| No. 6 | 24.70 | 24.26 | −1.78% | 10.40 | 10.44 | +0.33% | −0.133 | −0.133 | −0.22% | 0.44 | 6.78 |
| No. 7 | 24.83 | 23.38 | −5.83% | 10.50 | 10.28 | −2.14% | −0.131 | −0.127 | −3.64% | 0.67 | 6.93 |

**Fig. 9** Deformation of No. 1 and No. 7 propellers

It is important to note that since only unidirectional FSI tests have been performed, the obtained deformations are unrealistic since if the pressure distribution on the propeller blades changes due to the deformation, it will also affect the deformation.

Two-way FSI simulations would be needed to investigate this accurately, but due to lack of time, this will be part of a future study. The obtained deformation values show that the thinner the blade, the higher the deformation. It is worth noting that the stress (12.75 MPa) due to the deformation of the No. 3 propeller shown in Fig. 10 is comparable to the tensile strength (23.4 MPa) in the $x$-direction, so this is not a fortunate design, not to mention that the No. 3 propeller is very difficult to 3D-print due to the thin leading and trailing edges.

It is interesting to note that in almost all cases, the thrust generated on the propeller increased due to the deformation, which may be because the undeformed geometry is not optimized for this operating condition (e.g., $P/D$ 0.8 is too high) and the forward tilt of the propeller blades improves this. It is important to note here that torque also 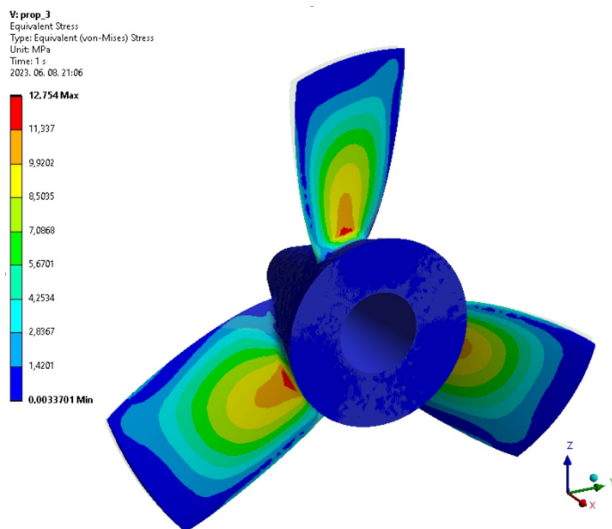increases due to deformation as thrust increases. A further observation to consider, illustrated in Fig. 11, is that the deformation of No. 5 propeller due to the geometry design reduces the gap between the nozzle and the propeller blades, which could lead to collision/damage in the worst case.

This is why the thrust of the overall thruster increased by 5.45%, an increase not only produced by the propeller. For the skewed propellers (No. 6 and No. 7), a reduction in thrust and torque is observed due to the twisting of the profiles at larger diameters. Overall, it can be stated that apart from extreme geometries (e.g., No. 3, No. 5, No. 7), the deformation of PLA propellers 3D-printed with FFF technology is not significant (max. 0.58 mm under the present design and material properties). CFD studies of the deformed geometries have shown that such deformation has no significant effect on the thrust and torque of the propeller and thruster.

As pointed out by [20], although the strength characteristics of FFF 3D-printed PLA propellers are adequate, ensuring the proper surface roughness is difficult. Without surface treatment, the torque demand of the propellers will be much higher, and the propeller's efficiency will be drastically reduced, even though the strength and geometric characteristics are satisfactory. If we look at the slicing of individual propellers, we can see that the amount of Rake and Skew strongly influences the arrangement of the layers and, thus the surface quality of the propeller blades.

## 7 Conclusion

This study investigated the in-service deformation of small PLA propellers 3D-printed using FFF technology and its effect on thrust with different input geometries. Seven different propeller geometries were investigated with the variable parameters of blade thickness, rake and skew. The results of the CFD and structural FEM simulations
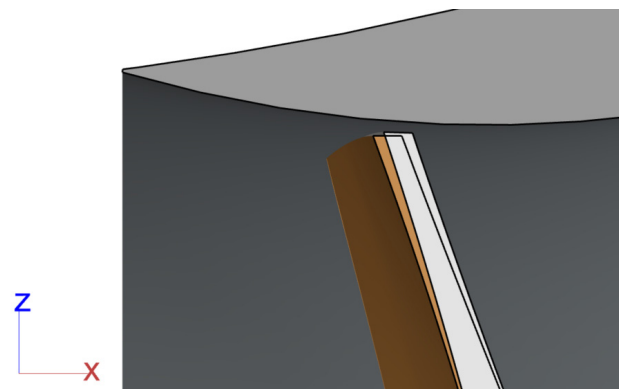


**Fig. 10** Equivalent (von-Mises) stress distribution of No. 3 propeller



**Fig. 11** Deformation of propeller No. 5 (Orange: undeformed; Grey: deformed)

showed that the deformation of small (diameter less than 100 mm) PLA propellers 3D-printed with FFF technology, rotating in a nozzle, is not significant, except for extreme geometries (e.g., thin blades, rake or skew greater than 10°). CFD studies of the deformed geometries have shown that the resulting deformation has no significant effect on the thrust and torque of the propeller and thruster. An important result is that the orthotropic material properties resulting from the FFF technology are not a problem for conventional geometries but rather the arrangement of the fibers formed during the lay-up process, which greatly impacts the surface roughness.

Future research plans include testing larger size and higher performance FFF 3D-printed propellers with bi-directional FSI simulations in multiple operating conditions. It would be good to investigate the impact on the propeller efficiency of the surface roughness due to the layers (e.g., using different layer thicknesses) or the different surface treatment methods used (e.g., sanding, epoxy filling, painting). In addition, real open water propeller experiments will be performed to validate the CFD model and further investigate different propellers. An additional motivation for additive manufacturing of propellers is that since CFD simulations of propellers always need to be validated in some way, it may be a cost-effective method to use 3D-printed propellers for experimental measurements. In this way, validated CFD models could be used to develop optimized propeller geometries that would greatly increase energy efficiency and sustainability and reduce pollution in shipping.

## Acknowledgement

## References

[1] Marini, S., Gjeci, N., Govindaraj, S., But, A., Sportich, B., Ottaviani, E., …, Papaelias, M. "ENDURUNS: An Integrated and Flexible Approach for Seabed Survey Through Autonomous Mobile Vehicles", Journal of Marine Science and Engineering, 8(9), 633, 2020.
https://doi.org/10.3390/jmse8090633

[2] Chang, H.-C., Hsu, Y.-L., Hung, S.-S., Ou, G.-R., Wu, J.-R., Hsu, C. "Autonomous Water Quality Monitoring and Water Surface Cleaning for Unmanned Surface Vehicle", Sensors, 21(4), 1102, 2021.
https://doi.org/10.3390/s21041102

[3] Sanjou, M., Shigeta, A., Kato, K., Aizawa, W. "Portable unmanned surface vehicle that automatically measures flow velocity and direction in rivers", Flow Measurement and Instrumentation, 80, 101964, 2021.
https://doi.org/10.1016/j.flowmeasinst.2021.101964

[4] Nicholson, J. W., Healey, A. J. "The Present State of Autonomous Underwater Vehicle (AUV) Applications and Technologies", Marine Technology Society Journal, 42(1), pp. 44–51, 2008.
https://doi.org/10.4031/002533208786861272

[5] Tanakitkorn, K., Phoemsapthawee, S. "Impacts of thruster configurations on the task performance of an unmanned surface vehicle", Ocean Engineering, 256, 111465, 2022.
https://doi.org/10.1016/j.oceaneng.2022.111465

[6] Li, C., Jiang, J., Duan, F., Liu, W., Wang, X., Bu, L., Sun, Z., Yang, G. "Modeling and Experimental Testing of an Unmanned Surface Vehicle with Rudderless Double Thrusters", Sensors, 19(9), 2051, 2019.
https://doi.org/10.3390/s19092051

[7] Raber, G. T., Schill, S. R. "Reef Rover: A Low-Cost Small Autonomous Unmanned Surface Vehicle (USV) for Mapping and Monitoring Coral Reefs", Drones, 3(2), 38, 2019.
https://doi.org/10.3390/drones3020038

[8] Stanway, M. J., Stefanov-Wagner, T. "Small-diameter ducted contrarotating propulsors for marine robots", In: OCEANS 2006, Boston, MA, USA, 2006, pp. 1–6. ISBN 1-4244-0114-3
https://doi.org/10.1109/OCEANS.2006.307030

[9] Joung, T.-H., Sammut, K., He, F., Lee, S.-K. "Shape optimization of an autonomous underwater vehicle with a ducted propeller using computational fluid dynamics analysis", International Journal of Naval Architecture and Ocean Engineering, 4(1), pp. 44–56, 2012.
https://doi.org/10.2478/IJNAOE-2013-0077

[10] Alam, K., Ray, T., Anavatti, S. G. "Design and construction of an autonomous underwater vehicle", Neurocomputing, 142, pp. 16–29, 2014.
https://doi.org/10.1016/j.neucom.2013.12.055

[11] Wang, Z., Wei, Z., Yu, C., Cao, J., Yao, B., Lian, L. "Dynamic modeling and optimal control of a positive buoyancy diving autonomous vehicle", Brodogradnja: An International Journal of Naval Architecture and Ocean Engineering for Research and Development, 74(1), pp. 19–40, 2023.
https://doi.org/10.21278/brod74102

[12] Ljulj, A., Slapnicar, V., Brigić, J. "Unmanned surface vehicle - Tritor", Brodogradnja: An International Journal of Naval Architecture and Ocean Engineering for Research and Development, 73(3), pp. 135–150, 2022.
https://doi.org/10.21278/brod73308

[13] Jo, W., Hoashi, Y., Aguilar, L., Postigo, M., Garcia-Bravo, J., Min, B.-C. "A low-cost and small USV platform for water quality monitoring", HardwareX, 6, e00076, 2019.
https://doi.org/10.1016/j.ohx.2019.e00076

[14] Sundar, A., Bain, S. "A Feasibility Study of Lightweight Polylactic Acid Fused Deposition Modeled Propeller Prototyping", Journal of Student Research, 11(3), pp. 1–13, 2022.
https://doi.org/10.47611/jsrhs.v11i3.2797

[15] Krmela, J., Bakošová, A., Krmelová, V., Sadjiep, S. "Drone Propeller Blade Material Optimization Using Modern Computational Method", In: 20th International Scientific Conference Engineering for Rural Development, Jelgava, Latvia, 2021, pp. 878–883.
https://doi.org/10.22616/ERDev.2021.20.TF199

[16] Toleos Jr., L. R., Luna, N. J. A. B. D., Manuel, M. C. E., Chua, J. M. R., Sangalang, E. M. A., So, P. C. "Feasibility Study for Fused Deposition Modeling (FDM) 3D-Printed Propellers for Unmanned Aerial Vehicles", International Journal of Mechanical Engineering and Robotics Research, 9(4), pp. 548–558, 2020.
https://doi.org/10.18178/ijmerr.9.4.548-558

[17] Wu, J., Dou, Y., Lv, H., Ma, C., Zhong, L., Xu, S., Han, X. "Thrust Characteristics of Ducted Propeller and Hydrodynamics of an Underwater Vehicle in Control Motions", Journal of Marine Science and Engineering, 9(9), 940, 2021.
https://doi.org/10.3390/jmse9090940

[18] Chen, C., Zou, L., Zou, Z., Guo, H. "Assessment of CFD-Based Ship Maneuvering Predictions Using Different Propeller Modeling Methods", Journal of Marine Science and Engineering, 10(8), 1131, 2022.
https://doi.org/10.3390/jmse10081131

[19] He, X. D., Hong, Y., Wang, R. G. "Hydroelastic optimisation of a composite marine propeller in a non-uniform wake", Ocean Engineering, 39, pp. 14–23, 2012.
https://doi.org/10.1016/j.oceaneng.2011.10.007

[20] Han, S., Lee, H., Song, M. C., Chang, B. J. "Investigation of Hydro-Elastic Performance of Marine Propellers Using Fluid-Structure Interaction Analysis", In: Proceedings of the ASME 2015 International Mechanical Engineering Congress and Exposition, Houston, TX, USA, 2015, V07AT09A038. ISBN 978-0-7918-5746-5
https://doi.org/10.1115/IMECE2015-51089

[21] Liang, L., Baoji, Z., Hao, Z., Hailin, T., Weijie, W. "Hydrodynamic performance optimization of marine propellers based on fluid-structure coupling", Brodogradnja: An International Journal of Naval Architecture and Ocean Engineering for Research and Development, 74(3), pp. 145–164, 2023.
https://doi.org/10.21278/brod74308

[22] Guan, G., Zhang, X., Wang, P., Yang, Q. "Multi-objective optimization design method of marine propeller based on fluid-structure interaction", Ocean Engineering, 252, 111222, 2022.
https://doi.org/10.1016/j.oceaneng.2022.111222

[23] Zhao, Y., Chen, Y., Zhou, Y. "Novel mechanical models of tensile strength and elastic property of FDM AM PLA materials: Experimental and theoretical analyses", Materials & Design, 181, 108089, 2019.
https://doi.org/10.1016/j.matdes.2019.108089

[24] Ficzere, P. "Experimental Dynamical Analysis and Numerical Simulation of the Material Properties of Parts Made by Fused Deposition Modelling Technologies", Periodica Polytechnica Transportation Engineering, 48(3), pp. 221–225, 2020.
https://doi.org/10.3311/PPtr.13947

[25] Yao, T., Ye, J., Deng, Z., Zhang, K., Ma, Y., Ouyang, H. "Tensile failure strength and separation angle of FDM 3D printing PLA material: Experimental and theoretical analyses", Composites Part B: Engineering, 188, 107894, 2020.
https://doi.org/10.1016/j.compositesb.2020.107894

[26] Bochnia, J., Blasiak, M., Kozior, T. "A Comparative Study of the Mechanical Properties of FDM 3D Prints Made of PLA and Carbon Fiber-Reinforced PLA for Thin-Walled Applications", Materials, 14(22), 7062, 2021.
https://doi.org/10.3390/ma14227062

[27] Alzyod, H., Ficzere, P. "Finite Element Modeling of Additive Manufacturing in Case of Metal Parts", Periodica Polytechnica Transportation Engineering, 50(4), pp. 330–335, 2022.
https://doi.org/10.3311/PPtr.19242

[28] The MathWorks, Inc. "MATLAB, (R2020b)", [computer program] The MathWorks, Inc., Natick, MA, USA, 2020.

[29] Carlton, J. S. "Chapter 3 - Propeller Geometry", In: Marine Propellers and Propulsion, Butterworth-Heinemann, 2019, pp. 29–46. ISBN 978-0-08-100366-4
https://doi.org/10.1016/B978-0-08-100366-4.00003-1

[30] Robert McNeel & Associates "Rhinoceros, (7.0)", [computer program] Robert McNeel & Associates, Seattle, WA, USA, 2020.

[31] ANSYS Inc. "ANSYS Fluent, (2021 R2)", [computer program] ANSYS, Inc., Canonsburg, PA, USA, 2021.

[32] ANSYS, Inc. "ANSYS Mechanical, (2021 R2)", [computer program] ANSYS, Inc., Canonsburg, PA, USA, 2021.

[33] Gonabadi, H., Yadav, A., Bull, S. J. "The effect of processing parameters on the mechanical characteristics of PLA produced by a 3D FFF printer", The International Journal of Advanced Manufacturing Technology, 111(3–4), pp. 695–709, 2020.
https://doi.org/10.1007/s00170-020-06138-4

[34] Huang, Y.-H., Lin. C.-Y. "Measurement of Orthotropic Material Constants and Discussion on 3D Printing Parameters in Additive Manufacturing", Applied Sciences, 12(13), 6812, 2022.
https://doi.org/10.3390/app12136812

[35] Monaldo, E., Ricci, M., Marfia, S. "Mechanical properties of 3D printed polylactic acid elements: Experimental and numerical insights", Mechanics of Materials, 177, 104551, 2023.
https://doi.org/10.1016/j.mechmat.2022.104551

[36] Torre, R., Brischetto, S. "Experimental characterization and finite element validation of orthotropic 3D-printed polymeric parts", International Journal of Mechanical Sciences, 219, 107095, 2022.
https://doi.org/10.1016/j.ijmecsci.2022.107095